


## On the physical association of *Fermi*-LAT blazars with their low-energy counterparts

RANIERE DE MENEZES <sup>1,2</sup>, RAFFAELE D'ABRUSCO,<sup>3</sup> FRANCESCO MASSARO,<sup>2,4,5,6</sup> DARIO GASPARRINI,<sup>7,8</sup> AND RODRIGO NEMMEN<sup>1</sup>

<sup>1</sup>*Universidade de São Paulo, Departamento de Astronomia, Rua do Matão, 1226, São Paulo, SP 05508-090, Brazil*

<sup>2</sup>*Dipartimento di Fisica, Università degli Studi di Torino, via Pietro Giuria 1, I-10125 Torino, Italy*

<sup>3</sup>*Center for Astrophysics — Harvard & Smithsonian, 60 Garden Street, Cambridge, MA 20138, USA*

<sup>4</sup>*Istituto Nazionale di Fisica Nucleare, Sezione di Torino, I-10125 Torino, Italy*

<sup>5</sup>*INAF-Osservatorio Astrofisico di Torino, via Osservatorio 20, 10025 Pino Torinese, Italy*

<sup>6</sup>*Consorzio Interuniversitario per la Fisica Spaziale (CIFS), via Pietro Giuria 1, I-10125, Torino, Italy*

<sup>7</sup>*Istituto Nazionale di Fisica Nucleare, Sezione di Roma “Tor Vergata”, I-00133 Roma, Italy*

<sup>8</sup>*Space Science Data Center - Agenzia Spaziale Italiana, Via del Politecnico, snc, I-00133, Roma, Italy*

(Received XXX, 2020; Revised XXX, 2020; Accepted 21 April 2020)

Submitted to ApJS

### ABSTRACT

Associating  $\gamma$ -ray sources to their low-energy counterparts is one of the major challenges of modern  $\gamma$ -ray astronomy. In the context of the Fourth *Fermi* Large Area Telescope Source Catalog (4FGL), the associations rely mainly on parameters as apparent magnitude, integrated flux, and angular separation between the  $\gamma$ -ray source and its low-energy candidate counterpart. In this work we propose a new use of likelihood ratio and a complementary supervised learning technique to associate  $\gamma$ -ray blazars in 4FGL, based only on spectral parameters as  $\gamma$ -ray photon index, mid-infrared colors and radio-loudness. In the likelihood ratio approach, we crossmatch the WISE Blazar-Like Radio-Loud Sources catalog with 4FGL and compare the resulting candidate counterparts with the sources listed in the  $\gamma$ -ray blazar locus to compute an association probability for 1138 counterparts. In the supervised learning approach, we train a random forest algorithm with 869 high confidence blazar associations and 711 fake associations, and then compute an association probability for 1311 candidate counterparts. A list with all 4FGL blazar candidates of uncertain type associated by our method is provided to guide future optical spectroscopic follow up observations.

*Keywords:* methods: statistical — galaxies: active — gamma rays: general

### 1. INTRODUCTION

The association of  $\gamma$ -ray sources with their low-energy counterparts is a long-standing challenge since the beginning of modern  $\gamma$ -ray astronomy (Fichtel et al. 1994). Its major underlying difficulty is related to the large positional uncertainty of  $\gamma$ -ray observations. Even in the era of the *Fermi* Large Area Telescope (LAT; Atwood et al. 2009), the positional uncertainty of  $\gamma$ -ray sources range from a couple of arcminutes up to  $\sim 1^\circ$  (Fermi-LAT Collaboration et al. 2019). Then, according to the recent release of the *Fermi*-LAT Fourth Source Catalog (4FGL; Fermi-LAT Collaboration et al. 2019),  $\sim 25\%$  of its sources lack an assigned low-energy counterpart and thus have uncertain nature. Although the fraction of unassociated  $\gamma$ -ray sources (UGSs) is still large, 4FGL presents a modest improvement in comparison with its previous releases, which had  $\sim 30\%$  of unassociated sources (Abdo et al. 2010; Nolan et al. 2012; Acero et al. 2015). The largest population of associated  $\gamma$ -ray sources is dominated by pulsars, pulsar wind nebulae and supernova remnant in the Galactic plane, and by blazars in the extragalactic sky (Fermi-LAT Collaboration et al. 2019)

Several studies searching for the counterparts of  $\gamma$ -ray sources have been performed in the past decade (Abdo et al. 2010; Nolan et al. 2012; Acero et al. 2015). Dedicated follow up observations at radio, infrared and X-rays allowed for the identification of potential counterparts for several *Fermi*-LAT sources, for which optical spectra were then collected to establish their nature (Massaro et al. 2015b, 2016; Crespo et al. 2016; Peña-Herazo et al. 2017; Marchesini et al. 2019; Peña-Herazo et al. 2019; de Menezes et al. 2020). Once a candidate counterpart is found, it can be considered in the association methods of the *Fermi*-LAT catalogs. All association methods used by the *Fermi*-LAT Collaboration (Fermi-LAT Collaboration et al. 2019) consist in computing the association probability (AP) based mainly on the angular separation between the center of the  $\gamma$ -ray source and the position of its candidate counterpart, thus being mostly a geometrical approach and neglecting physical properties of candidate counterparts, such as colors, spectral shape and radio-loudness, to name a few. When a candidate counterpart has AP > 80% in 4FGL, the source is considered associated.

In this work we propose two different association procedures, both independent of angular separation and relying mainly on the  $\gamma$ -ray-mid-infrared connection of candidate blazar counterparts selected from the WISE Blazar-Like Radio-Loud Sources catalog (WIBRaLS; D’Abrusco et al. 2019). WIBRaLS is a catalog of radio-loud candidate blazars whose WISE mid-infrared (MIR) colors are selected to be consistent with MIR colors of confirmed  $\gamma$ -ray emitting blazars (Massaro et al. 2011; D’Abrusco et al. 2012). We compute the APs with two different methods: i) the likelihood ratio (LR; Sutherland & Saunders 1992), already adopted by the *Fermi*-LAT Collaboration, but with a different setup; and ii) a random forest algorithm (RF; Breiman 2001). By assigning an AP to each candidate counterpart, we can schedule/program future optical spectroscopic follow-ups on these results, prioritizing those targets with higher AP.

Computing an AP for each counterpart candidate is crucial because all methods used to select candidate blazars are statistical in nature and do not take into account the specific  $\gamma$ -ray properties of each *Fermi* source to be associated but only collective features of a population of sources (in our case, the  $\gamma$ -ray emitting confirmed blazars in the blazar locus. See §2). Thus, association methods bridge the gap between collective behavior and each specific case, giving an intra-source prioritization – should there be multiple candidates for the same  $\gamma$ -ray source – and an inter-source prioritization to maximize the effectiveness of spectroscopic follow-ups.

Machine learning techniques have been used before in the context of *Fermi*-LAT catalogs to i) predict the spectral class of UGSs (Doert & Errando 2014; Parkinson et al. 2016; Lefaucheur & Pita 2017; Salvetti et al. 2017) based only on the  $\gamma$ -ray properties available in the Second and Third *Fermi* Source Catalogs (2FGL and 3FGL, respectively; Nolan et al. 2012; Acero et al. 2015); ii) predict the nature of blazar candidates of uncertain type (BCUs; Hassan et al. 2012; Chiaro et al. 2016; Kovačević et al. 2019); iii) and even for spotting candidates of dark matter Galactic subhalos (Mirabal et al. 2012). This is the first time, however, that machine learning is used to associate *Fermi*-LAT sources with their low-energy counterparts.

The idea underlying this work is that  $\gamma$ -ray blazars have some specific radio-MIR characteristics which can tell them between, e.g., two counterpart candidates lying in the same elliptical uncertainty region of a  $\gamma$ -ray source. Indeed, some sources associated in 4FGL have a very high AP with counterparts that are not the closest ones if compared with sources listed in the latest version of WIBRaLS (D’Abrusco et al. 2019). This can happen simple because the latest version of WIBRaLS was not taken into account when associating 4FGL sources, but highlights a possible bias in a method that associate sources based mainly on angular separation: if the real  $\gamma$ -ray source counterpart is not listed in one of the catalogs used by the association algorithms, then the method will simply choose the closest candidate.

The paper is organized as follows. In §2 and §3 we describe the samples used to carry out our analysis, providing basic details on both WIBRaLS and 4FGL. In §4 and §5 we describe the adopted methods followed by the achieved results in §6 and §7. We conclude and summarize our work in §8. The WISE magnitudes are in the Vega system and are not corrected for the Galactic extinction, since, as shown in D’Abrusco et al. (2014), such correction only affects the magnitude at 3.4  $\mu$ m for sources lying close to the Galactic plane and it ranges between 2% and 5% of the magnitude, thus not affecting significantly the results. WISE bands are indicated as W1, W2, W3 and W4, and correspond respectively to the nominal wavelengths at 3.4, 4.6, 12, and 22  $\mu$ m, while the colors are defined as  $c_{12} = W1 - W2$ ,  $c_{23} = W2 - W3$  and  $c_{34} = W3 - W4$ . The adopted MIR radio-loudness parameter is defined as  $q_{22} = \log(S_{22\mu m}/S_{radio})$ , where  $S_{22\mu m}$  is the flux density in the WISE W4 band, and  $S_{radio}$  is the radio flux density at 1.4 GHz or at 843 MHz, depending on the radio survey in which the WIBRaLS radio counterpart is identified (see D’Abrusco et al. 2019, for more details).

## 2. SAMPLES USED FOR THE LIKELIHOOD RATIO METHOD

We apply the LR method to all 1311 sources listed in 4FGL with at least one counterpart in WIBRaLS, comparing their MIR colors and radio-loudness with those of the  $\gamma$ -ray blazars lying within the blazar locus (D’Abrusco et al. 2013).

The blazar locus is defined by a sample of confirmed *Fermi*-LAT blazars listed in Roma-BZCAT (Massaro et al. 2015a) and associated with WISE counterparts detected in all four filters W1, W2, W3 and W4. The locus is modeled in a three-dimensional space generated by the principal components of the MIR color-color-color distribution and describes the typical MIR colors of  $\gamma$ -ray blazars, thus being ideal for our purposes (see, e.g., D’Abrusco et al. 2013, 2019).

## 3. SAMPLES USED FOR THE SUPERVISED LEARNING METHOD

The training set of supervised learning algorithms needs to be representative of the expected distribution of outcomes in the test set, or the sample on which the trained algorithm will be applied. In this case, we train a RF algorithm by gathering high-confidence associations and not-associated (fake) counterparts. We do it by selecting all associated sources in 4FGL having a counterpart in WIBRaLS and with  $\gamma$ -ray statistical significance above  $10\sigma$ . Such high confidence  $\gamma$ -ray detections tend to have smaller error ellipses, and for this reason they are easier to correctly associate with low-energy counterparts. The final number of high confidence associations in the training set was 869. The fake associations were selected as the WIBRaLS sources not associated in 4FGL but lying within  $0.5^\circ$  from 4FGL sources that are already associated with a low-energy counterpart, resulting in a total of 711 fake counterparts for the training sample. It is possible that a few of these fake associations are the real counterparts of the  $\gamma$ -ray sources.

The panels in Figure 1 show the differences between high confidence associations (contours) and fake associations (orange dots) in the training sample. Based on these  $\gamma$ -ray-MIR characteristics, supervised learning algorithms can be trained to tell how likely a WIBRaLS source is associated as the counterpart of a  $\gamma$ -ray source. Once trained, we applied the RF method to a test sample made of the 1311 4FGL-WIBRaLS crossmatches, the same sample used in the LR method.

## 4. THE LIKELIHOOD RATIO METHOD

The LR technique was first used in the context of source association by Richter (1975) and has been introduced and developed to look for possible counterparts among faint radio, infrared and X-ray sources (Wolstencroft et al. 1986; Sutherland & Saunders 1992; Masci et al. 2001). In the context of *Fermi*-LAT, the LR between a candidate counterpart  $i$  within the error ellipse of a 4FGL source  $j$  is computed as (Ackermann et al. 2011; The *Fermi*-LAT collaboration 2019):

$$LR_{ij} = \frac{e^{-r_{ij}^2/2}}{NA}, \quad (1)$$

where  $r_{ij} = \theta/(\sigma_i^2 + \sigma_j^2)^{1/2}$  is the normalized angular separation between the  $\gamma$ -ray source  $j$  and candidate counterpart  $i$ , with  $\theta$  being the angular separation between the counterpart and the center of the  $\gamma$ -ray source,  $\sigma_i$  being the low-energy positional uncertainty and  $\sigma_j \equiv \sigma_{95\%}/2.4477$  being the normalized geometric mean of the semi-major and semi-minor axes of the 95% 4FGL confidence error ellipse.  $N$  is the surface density of objects brighter than the candidate  $i$  and  $A$  is the solid angle encompassed by the 95% confidence LAT error ellipse. Below we modify this method by taking into account only spectral properties of the candidate counterparts, as MIR colors and radio-loudness, and comparing these properties with what is expected for  $\gamma$ -ray blazars lying in the blazar locus (D’Abrusco et al. 2013). In §6.1 we add a dependence on the angular separation to this method to measure the impact of angular separation in our results.

The LR method we adopt to estimate the AP is a modification of the LR method described in Sutherland & Saunders (1992) and Ackermann et al. (2011). The adopted steps are as follows.

1. We crossmatch WIBRaLS with 4FGL to create the list of all  $\gamma$ -ray blazar candidates that lie within the positional uncertainty region at 95% level of confidence of each *Fermi*-LAT object. With a total of 1311 potential counterparts, the result of this crossmatch correspond to all of the 4FGL candidate counterparts listed in WIBRaLS.
2. For each 4FGL source, we consider the  $\gamma$ -ray photon index interval  $\Delta\Gamma = [\Gamma - \sigma_\Gamma, \Gamma + \sigma_\Gamma]$ , where  $\sigma_\Gamma$  is the uncertainty on the photon index as listed in 4FGL. Then, given the correlations between  $\Gamma$ , the MIR colors  $c_{12}$  and  $c_{34}$ , and the MIR radio-loudness  $q_{22}$  for the blazars in the  $\gamma$ -ray blazar locus (D’Abrusco et al. 2012), we

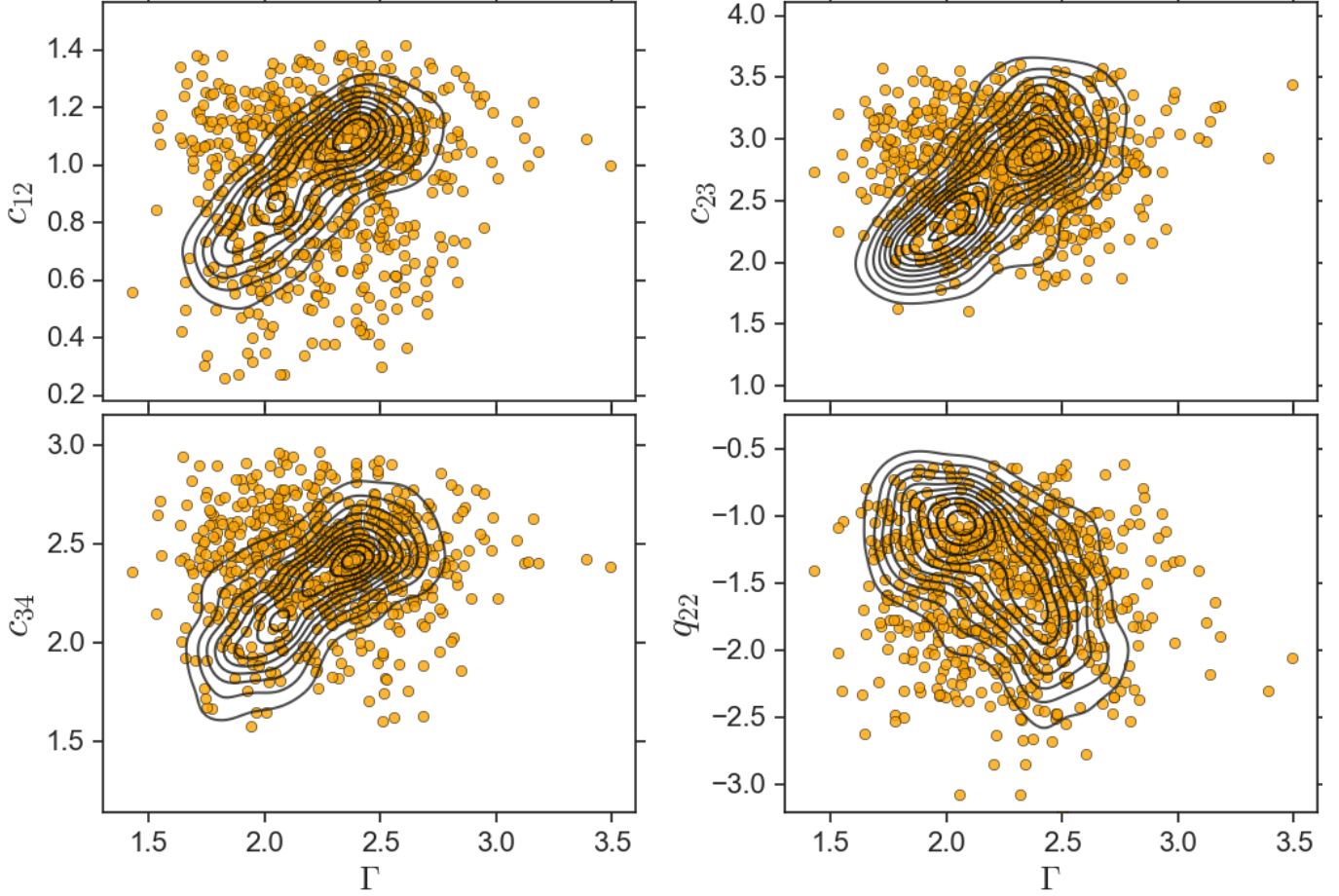


**Figure 1.** Training sample for the RF algorithm. The contours represent the distribution of the 869 high confidence associations, while the orange dots represent the fake associations. The spectral parameters for the training sample are shown in terms of the  $\gamma$ -ray photon index,  $\Gamma$ , the three MIR colors  $c_{12}$ ,  $c_{23}$  and  $c_{34}$  (as defined in the last paragraph of §1) and the MIR radio-loudness  $q_{22}$ .

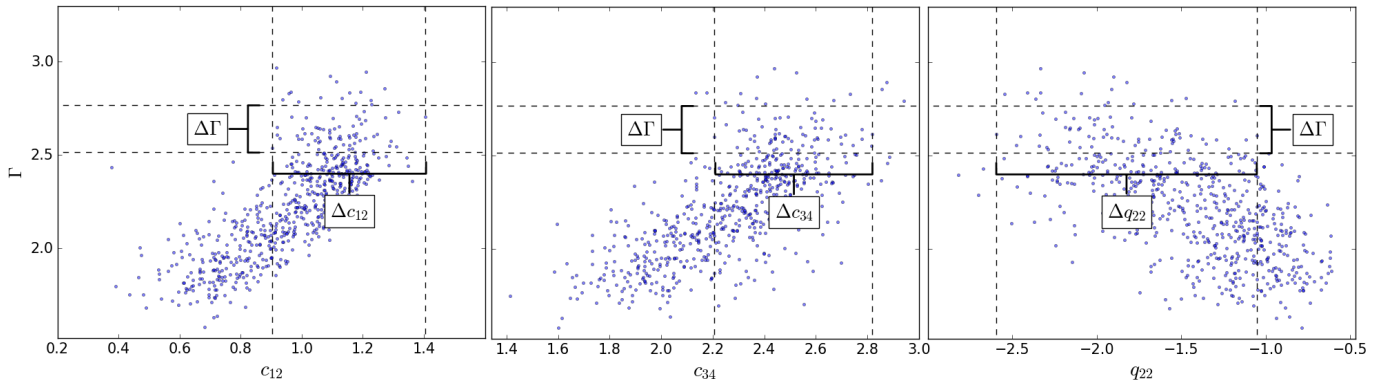


**Figure 2.** Region selected in the blazar locus for a source with  $\gamma$ -ray photon index  $\Gamma = 2.65 \pm 0.10$ . Given an interval  $\Delta\Gamma$ , only the sources within the ranges  $\Delta c_{12}$ ,  $\Delta c_{34}$  and  $\Delta q_{22}$  can be selected as possible counterparts of  $\gamma$ -ray sources.

select from WIBRaLS only those sources with parameters within the blazar locus ranges  $\Delta c_{12} = [c_{12}^{min}, c_{12}^{max}]$ ,  $\Delta c_{34} = [c_{34}^{min}, c_{34}^{max}]$  and  $\Delta q_{22} = [q_{22}^{min}, q_{22}^{max}]$  corresponding to the  $\Delta\Gamma$  interval, as shown in Figure 2. This step reduces the total number of candidate counterparts from 1311 to 1138.

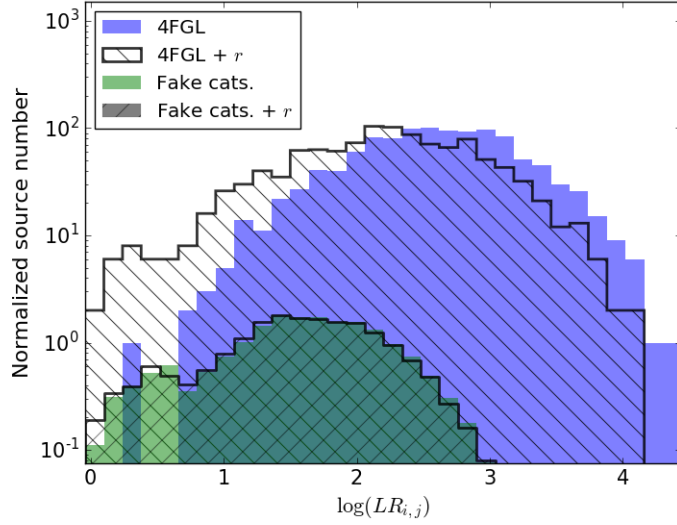


**Figure 3.** Distribution of the  $\log(LR_{i,j})$  for the crossmatches between WIBRaLS and 4FGL ( $G_{\text{real}}$ ), in blue; and average distribution for the crossmatches between WIBRaLS and the fake  $\gamma$ -ray catalogs ( $\langle G_{\text{fake}} \rangle$ ), in green. The hatched histograms represent the same distributions when taking angular separation,  $r$ , into account with the exponential behaviour shown in Equation 1.

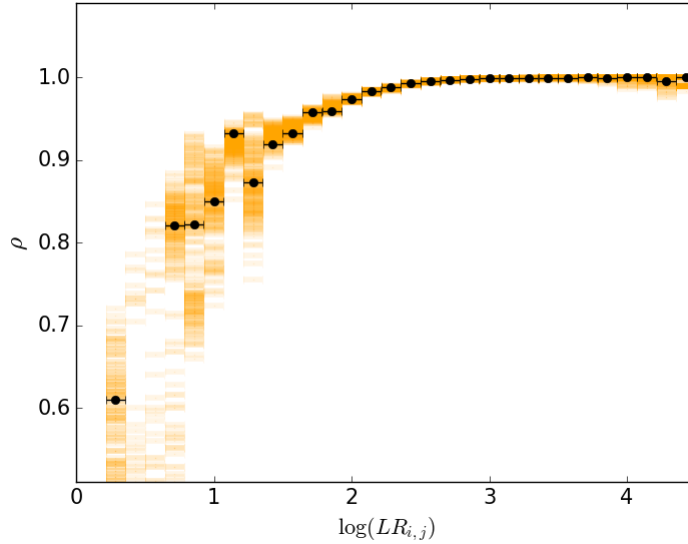


**Figure 4.** The reliability  $\rho$  derived from the LR method as function of  $\log(LR_{i,j})$ . The black dots are the points adopted in this work, while the orange shadow represents the uncertainty region due to different choices of radii when computing the local surface density  $N(\Delta c_{12}, \Delta c_{34}, \Delta q_{22})$ . In the region  $\log(LR_{i,j}) > 1.5$ , the impact of choosing different radii is negligible.

3. For each MIR counterpart  $i$  of a 4FGL source  $j$  we compute the LR using the following equation:

$$\log LR_{i,j} = \log \left[ \frac{1}{2\pi\sigma_1\sigma_2} \frac{Q(\Delta c_{12}, \Delta c_{34}, \Delta q_{22})}{N(\Delta c_{12}, \Delta c_{34}, \Delta q_{22})} \right],$$

where  $Q(\Delta c_{12}, \Delta c_{34}, \Delta q_{22})$  is the probability to find a WIBRaLS source with MIR colors and radio-loudness within the ranges  $\Delta c_{12}$ ,  $\Delta c_{34}$  and  $\Delta q_{22}$  over the entire WIBRaLS catalog (i.e., it is the ratio between the total number of sources lying within the specified intervals and the total number of WIBRaLS sources), and  $N(\Delta c_{12}, \Delta c_{34}, \Delta q_{22})$  is the local surface density of WIBRaLS sources within a circle of  $8^\circ$  radius centered in the 4FGL source and having MIR colors and radio-loudness within the specified ranges (i.e., it is the surface density

of the background objects at the appropriate Galactic latitude). The positional uncertainty errors of the 95% confidence regions of 4FGL sources are given by  $\sigma_1$  and  $\sigma_2$ . Angular separation between the  $\gamma$ -ray source and its counterpart is not taken into account.

4. To compute the AP based on the LR calculated above, we first generate 500 fake  $\gamma$ -ray catalogs by shifting the sky positions of each 4FGL source by a random value between  $0.3^\circ$  and  $3^\circ$  in a random direction of the sky. These small shifts in R.A. and Dec. guarantee that we preserve the inhomogeneity of the  $\gamma$ -ray sky, which has more sources concentrated towards the Galactic plane. We then repeat steps 2 and 3 above for all matches between the fake sources (belonging to the 500 generated catalogs) and WIBRaLS sources to compute the average distribution function ( $\langle G_{\text{fake}}(LR_{i,j}) \rangle$ ) of fake  $\log LR_{i,j}$ . The  $\log LR_{i,j}$  distributions for the real and fake matches are shown in blue and green, respectively, in Figure 3. As a matter of comparison, we overplot the  $\log LR_{i,j}$  distributions when adding the exponential dependence of angular separation,  $r$ , shown in Equation 1, to our method (hatched distributions).
5. We then compare the real and the fake distributions of  $\log LR_{i,j}$  to determine the reliability for the real associations by computing:

$$\rho(LR_{i,j}) = 1 - \frac{\langle G_{\text{fake}}(LR_{i,j}) \rangle}{G_{\text{real}}(LR_{i,j})},$$

where  $\langle G_{\text{fake}}(LR_{i,j}) \rangle$  is the average  $\log LR_{i,j}$  distribution for fake catalogs and  $G_{\text{real}}(LR_{i,j})$  is the  $\log LR_{i,j}$  distribution for the real  $\gamma$ -ray source catalog, as shown in Figure 3. The reliability,  $\rho$ , computed according to this equation represents an approximate measurement of the AP for a potential counterpart having a given  $\log LR_{i,j}$ . In Figure 4 we show the dependence of  $\rho$  on  $\log(LR_{i,j})$ . Some fluctuations are observed for  $\log(LR_{i,j}) < 1.5$ , but the overall behaviour of the curve is clear: for  $\log(LR_{i,j}) > 1.5$ , basically all counterpart candidates have very high ( $> 95\%$ ) APs. The orange shadow in Figure 4 represent the uncertainty region caused by choosing different radii when computing the local surface density (see step 3 above). This region was generated by ranging the radii from  $3.5^\circ$  up to  $15^\circ$  in 200 linearly spaced intervals. We observe that, in the region defined by  $\log(LR_{i,j}) > 1.5$ , the APs do not really depend on how we choose the background region radius.

The APs obtained with this method range from 60% to 100%. Among the sources listed as identified in 4FGL—those for which the association to the low-energy counterpart is guaranteed—the APs are always above 99%.

## 5. THE RANDOM FOREST METHOD

In the context of supervised learning algorithms, we use a RF (Breiman 2001) to compute the AP of 4FGL counterparts. The RF method is an ensemble classifier that uses decision trees as building blocks for classification (James et al. 2013). For classifying a new object, each tree in the forest chooses one class and, by aggregating the predictions of all decision trees, the RF makes a final prediction based on the choice made by the majority of the trees, thus improving the predictive capability and reducing the tendency of standard decision trees to overfit the training sample.

We train and estimate the accuracy of the RF method with the sample described in §3 using cross-validation: the RF algorithm has been trained with 10 subsets, each containing 90% of the training sample (where the sources are randomly chosen), and testing it on the complementary 10 subsets containing 10% of the training sample, in a way that the final accuracy of  $78.2\% \pm 3.3\%$  is simply the average ratio of correctly predicted observations to the total observations. The following attributes listed in 4FGL and WIBRaLS were used during the learning process:  $\gamma$ -ray power law photon index  $\Gamma$ , WISE colors  $c_{12}$ ,  $c_{23}$ , and  $c_{34}$ , and radio-loudness  $q_{22}$  computed with respect to the infrared flux in band W4. We tested several other parameters available in 4FGL and WIBRaLS, as  $\gamma$ -ray variability index and ratios between  $\gamma$ -ray flux densities (power law and logparabola spectral models) and radio flux density, but all of them presented a negligible impact on the results, with improvements in the algorithm accuracy of  $\sim 3\%$  in the best case (i.e.,  $\gamma$ -ray variability index), and sometimes only adding noise. Among the used parameters, the one with largest impact in the accuracy when combined with  $\Gamma$  is  $c_{12}$ , followed by  $c_{34}$ ,  $q_{22}$  and  $c_{23}$ , respectively. As discussed in §1, we are neglecting angular separation between the center of the  $\gamma$ -ray sources and the position of the MIR sources listed in WIBRaLS, as we are proposing an association method that relies only on spectral properties.

We use the RF classifier available in the Python library `sklearn` (Pedregosa et al. 2011). The code fits several decision trees on sub-samples of the dataset and average them to improve the predicted accuracy and prevent overfitting. To guarantee the stability of our results, we use 5000 trees and let the nodes grow until all leaves contain less

than the minimum number of samples required to split an internal node. The APs obtained with the RF algorithm range from 5% to 100% and the lowest AP obtained for blazars listed as identified in 4FGL (all of them included in the training sample) is 70%.

## 6. RESULTS FROM THE LIKELIHOOD RATIO APPROACH

The total number of associations with  $AP > 99\%$  (i.e., as high as the AP obtained for the identified 4FGL sources. See §4) is 743 out of the 1138 original 4FGL-WIBRaLS crossmatches within the intervals  $\Delta_{c_{12}}$ ,  $\Delta_{c_{34}}$  and  $\Delta_{q_{22}}$ . This number increases to 1051 when considering counterparts with  $AP > 95\%$ . Among all the 1138 sources for which we compute an AP, 283 are associated in 4FGL as BCUs, 473 as BL Lacs, 350 as flat spectrum radio quasars (FSRQs) and the rest of them are divided into a few non-blazar extragalactic and unknown objects. We found 5 UGSs with a counterpart in WIBRaLS and with APs ranging from 93% up to 99%. The BCUs and UGSs associated here—specially those with APs as high as the identified 4FGL sources—are promising targets for future optical spectroscopic follow up missions. In fact, optical spectroscopic observations for some of them are available in [de Menezes et al. \(2020\)](#) and [Peña-Herazo et al. \(2020, in prep.\)](#), where all of the sources have blazar-like optical spectra. All BCUs and UGSs associated here are listed in Tables 2 and 3 in Appendix A.

Among the  $\gamma$ -ray sources associated here (with any AP), 22 of them have different counterparts in 4FGL which are not listed in WIBRaLS (see Table 1). Probably due to the exponential dependence with angular separation (see Eq. 1) adopted in 4FGL, the 22 counterparts listed in 4FGL are generally closer to the center of the  $\gamma$ -ray sources than the WIBRaLS counterparts selected based on MIR colors. Furthermore, 165 of the 1138 WIBRaLS counterpart candidates are not associated by the LR method adopted in 4FGL. These sources were associated in 4FGL mainly via the Bayesian method ([Fermi-LAT Collaboration et al. 2019](#)). Additionally, no correlation is observed between the APs computed here and the APs computed with the LR method adopted in 4FGL, indicating that the methods are completely independent.

### 6.1. Considering angular separation

When we consider angular separation (with an exponential dependence as shown in Equation 1) together with WISE MIR colors and  $q_{22}$ , the LR distributions look like the hatched histograms in Figure 3. As the distributions are very similar, the APs resulting when considering angular separation are also similar. The total number of associated counterparts in this case is 580 with  $AP > 99\%$ , or 1071 when considering  $AP > 95\%$ . Furthermore, all sources with  $AP < 95\%$  have low  $\gamma$ -ray statistical significance ( $< 10\sigma$ ), which generally implies in large positional and  $\gamma$ -ray photon index errors.

In the upper panel of Figure 5 we compare the APs obtained with the LR method developed here with those obtained with the LR adopted in 4FGL. In the bottom panel we show the same comparison, but when taking into account the angular separation,  $r$ , in the LR method. In both cases our method tend to give higher APs.

## 7. RESULTS FROM THE RANDOM FOREST APPROACH

We found a total of 960 associations with  $AP > 70\%$  (i.e., in the same range of the identified 4FGL sources. See §5) out of 1311 test sources (see §3). Furthermore, the number of counterparts with  $AP > 50\%$  increases to 1109. Due to the low accuracy presented by the RF method (see §5), we use these results only as a comparison to the LR method described in the previous section. The APs for the BCUs and UGSs associated with the RF are shown in Tables 2 and 3 in Appendix A.

When comparing the APs obtained with the RF algorithm and those obtained with the LR methods used here and in 4FGL, we found no significant correlation, although the APs computed with the RF approach tend to be smaller and distributed over a larger range. The major difference between both methods is the way we feed the two algorithms with the data. In Figure 1 it is clear that several fake associations (orange dots) occupy the same region as the high confidence associations, thus counterparts lying within the high confidence association region (black contours) still have a high chance of being a fake association in the RF approach. The same does not happen with the LR method. Furthermore, based on how we defined the training set and the fake associations, we are solving an intrinsically more complicated task with the RF approach than with the LR method.

## 8. DISCUSSION AND CONCLUSIONS

4FGL name	Association WIBRaLS	Association 4FGL	AP LR WIB	AP LR 4FGL
J0119.9+4053	J011947.90+405418.4	CRATES J012018+405314	0.97	–
J0211.1-0646	J021116.95-064419.9	LEDA 1029376	0.99	0.96
J0237.7+0206	J023737.97+020742.5	PKS 0235+017	0.93	–
J0402.9+6433	J040254.43+643510.0	1RXS J040301.8+643446	0.99	0.83
J0640.9-5204	J064111.26-520232.2	ERC217 G261.25-22.62	0.99	–
J0725.6-3530	J072548.16-353041.8	NVSS J072547-353039	0.99	–
J0801.3-0617	J080141.07-060535.2	CRATES J080140-054037	0.61	–
J0807.7-1206	J080730.69-120608.9	CRATES J080736.06-120745.9	0.93	0.92
J1122.0-0231	J112213.71-022914.0	2QZ J112156-0229	0.96	–
J1136.3-0501	J113547.40-050804.8	NVSS J113607-050156	0.86	–
J1145.7+0453	J114631.75+045819.2	PKS 1142+052	0.93	0.89
J1300.4+1416	J130020.92+141718.4	OW 197	0.96	0.95
J1305.3+5118	J130645.87+511655.0	IERS B1303+515	0.83	–
J1516.8+2918	J151641.71+291816.5	RGB J1516+293	0.97	0.89
J1518.6+0614	J151847.70+061259.0	TXS 1516+064	0.96	0.96
J1550.8-1750	J155053.18-175618.4	TXS 1548-177	0.97	0.88
J1734.0+0805	J173510.44+080831.0	2MASS J17340287+0805237	0.86	0.83
J1807.1+2822	J180712.91+282059.5	WISE J180634.08+281908.0	0.86	–
J1953.0-7025	J195306.71-702428.7	PKS 1947-705	0.99	0.96
J2110.2-1021	J211038.30-103337.2	PKS 2107-105	0.86	0.95
J2209.8-5028	J221040.80-502652.5	PMN J2210-5030	0.96	–
J2329.7-2118	J232940.19-211345.0	PKS 2327-215	0.97	0.88

**Table 1.** List of sources with associations provided with the LR method developed here and having a different association in 4FGL. As expected, most (but not all) of the associations listed in 4FGL are closer to the  $\gamma$ -ray emission center than the WIBRaLS candidate counterparts selected based on MIR colors. Starting from the left side, the columns are i) the name of the  $\gamma$ -ray source in 4FGL, ii) the WISE name of the WIBRaLS candidate counterpart selected based on MIR colors, iii) the candidate counterpart listed in 4FGL, iv) the AP obtained with the LR method developed here, and v) the AP obtained with the LR used in 4FGL.

Associating  $\gamma$ -ray sources with their low-energy counterparts is challenging. Given the absence of multiwavelength monitoring and optical spectroscopic data within the error ellipses of many 4FGL sources, we have to recur to statistical methods when associating  $\gamma$ -ray sources to their counterparts.

In this work we propose an alternative to the LR association method adopted by the *Fermi*-LAT Collaboration (Fermi-LAT Collaboration et al. 2019). Here, the APs are independent of angular separation and apparent magnitude, and rely only on spectral parameters such as MIR colors and radio-loudness. As a complementary association method, we trained a RF algorithm to associate  $\gamma$ -ray sources to their counterparts. Both methods, however, are suited only for associating blazar candidates to  $\gamma$ -ray sources. Other types of  $\gamma$ -ray sources, like pulsars and starburst galaxies (to name a few), can not be directly associated with the proposed methods.

In the LR method adopted here we naturally loose some true blazar associations which have MIR colors just outside the blazar locus (i.e., the region of the WISE color-color-color diagram populated by confirmed  $\gamma$ -ray blazars). The sources associated here, however, are very good  $\gamma$ -ray blazar candidates and excellent targets for future optical spectroscopic follow ups. Furthermore, as all sources in WIBRaLS are radio-loud with respect to the  $q_{22}$  parameter (D’Abrusco et al. 2019), it is likely to find many BL Lac-galaxy dominated among the sources excluded by our method. It is really unlikely that these sources have no sign of nuclear activity, as the presence of non-AGNs in WIBRaLS is estimated to be  $< 5\%$  (de Menezes et al. 2019). The results from our analysis are as follows.

- The total number of associations computed with the LR method is 743 with AP  $> 99\%$ , or 1051 associations with AP  $> 95\%$ . We associate a total of 283 BCUs and 5 UGSs (listed in Tables 2 and 3 in Appendix A).
- Adding a dependence on angular separation to the LR method do not change significantly the results, indicating that WIBRaLS sources are generally in good positional agreement with 4FGL sources.



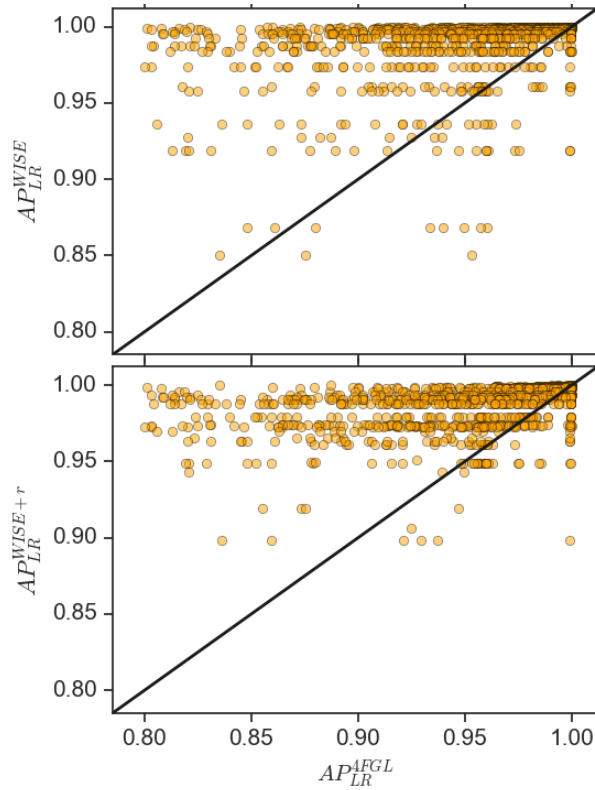


**Figure 5.** Comparison between the APs obtained with our LR method neglecting (upper panel) and considering (bottom panel) angular separation and the APs obtained with the LR method used in 4FGL. The APs computed by our method tend to be higher than those listed in 4FGL paper.

- A supervised learning method is used for the first time to associate counterparts to  $\gamma$ -ray sources. As the performance of the algorithm is  $\sim 80\%$ , the results derived from this method are considered complementary to those obtained with the LR method and should not be interpreted as giving definitive associations to 4FGL sources.

This is the first work where spectral properties of blazars are used to associate  $\gamma$ -ray sources to their low-energy counterparts. Previous methods rely basically on parameters like apparent magnitude and angular separation between the  $\gamma$ -ray source center and the position of its candidate counterpart.

The lists of BCUs and UGSs available in Appendix A give an excellent opportunity for testing the LR method presented here. In tables 2 and 3, the targets are sorted alphabetically and can be prioritized by choosing those with higher APs. Optical spectroscopy follow ups of these targets may be crucial to test if the association based on MIR colors is indeed an appropriate approach.

4FGL name	WISE name	LR WISE	RF	Bayesian	LR 4FGL
J0001.6-4156	J000132.74-415525.2	0.99	0.97	1.0	0.85
J0008.0-3937	J000809.17-394522.8	0.87	0.61	0.92	0.88
J0010.8-2154	J001053.64-215704.2	0.96	0.42	0.99	0.95
...	...	...	...	...	...
J1238.1-4541	J123806.03-454129.6**	0.99	1.0	1.0	0.94
J1239.4+0728	J123924.58+073017.2*	1.0	0.96	1.0	0.94
...	...	...	...	...	...

**Table 2.** BCUs associated by the LR method based only on spectral parameters. The BCUs listed here are good targets for future optical spectroscopic follow ups. In the first two columns we have the names of the  $\gamma$ -ray source and its WISE counterpart. The last four columns show the APs as given by the LR and RF methods in this work and by the Bayesian and LR methods used in 4FGL. Sources tagged with “\*” and “\*\*” are confirmed blazars, with optical spectra available in [de Menezes et al. \(2020\)](#) and [Peña-Herazo et al. \(2020, in prep\)](#), respectively. The full version of this table is available in the online material.

## ACKNOWLEDGMENTS

This work was supported by FAPESP (Fundação de Amparo à Pesquisa do Estado de São Paulo) under grants 2016/25484-9, 2018/24801-6 (R.M.) and 2017/01461-2 (R.N.). The work of F.M. is partially supported by the “Departments of Excellence 2018-2022” Grant awarded by the Italian Ministry of Education, University and Research (MIUR) (L. 232/2016) and made use of resources provided by the Compagnia di San Paolo for the grant awarded on the BLENV project (S1618\_L1.MASF\_01) and by the Ministry of Education, Universities and Research for the grant MASF\_FFABR\_17.01. F.M. also acknowledges financial contribution from the agreement ASI-INAF n.2017-14-H.0 while A.P. the financial support from the Consorzio Interuniversitario per la Fisica Spaziale (CIFS) under the agreement related to the grant MASF\_CONTR\_FIN\_18.02. R.D’A. is supported by NASA contract NAS8-03060 (Chandra X-ray Center). This investigation is supported by the National Aeronautics and Space Administration (NASA) grants GO6-17081X and GO9-20083X. We thank the anonymous referee for the constructive comments allowing us to improve the manuscript.

In this publication we made use of data products from the Wide-field Infrared Survey Explorer, which is a joint project of the University of California, Los Angeles, and the Jet Propulsion Laboratory/California Institute of Technology, funded by the National Aeronautics and Space Administration. We also used TOPCAT<sup>1</sup> ([Taylor 2005](#)) and astropy<sup>2</sup> ([Astropy Collaboration et al. 2013, 2018](#)) for preparation and manipulation of the data.

## APPENDIX

### A. LIST OF TARGETS FOR OPTICAL SPECTROSCOPIC FOLLOW UP

A list with all BCUs associated with the LR method is provided in Table 2, where the sources are promising targets for future optical spectroscopic follow ups. The columns are the name of the source in  $\gamma$ -rays and MIR, the AP obtained with the LR method developed here, the AP obtained with the RF approach, the AP obtained with the Bayesian method used in 4FGL and the AP computed with the LR method based on angular distance as in 4FGL. Similarly, Table 3 lists the 5 UGSs described in §6 and §7 and their APs.

## REFERENCES

- Abdo, A. A., Ackermann, M., Ajello, M., et al. 2010, The Astrophysical Journal Supplement Series, 188, 405
- Ajero, F., Ackermann, M., Ajello, M., et al. 2015, The Astrophysical Journal Supplement Series, 218, 23
- Ackermann, M., Ajello, M., Allafort, A., et al. 2011, The Astrophysical Journal, 743, 171

<sup>1</sup> <http://www.star.bris.ac.uk/~mbt/topcat/>

<sup>2</sup> <https://www.astropy.org/index.html>

4FGL Name	WISE name	LR WISE	RF
J0202.4+2943	J020239.70+294325.0	0.99	0.75
J0620.7-5034	J062046.13-503350.9	0.97	0.68
J1028.1-3550	J102751.56-355210.7	0.98	0.31
J1309.3+8035	J130628.16+803142.3	0.93	0.61
J2013.9-8717	J201440.97-871707.8	0.98	0.90

**Table 3.** UGSs associated by the LR method. These sources are good targets for future optical spectroscopic follow ups. In the first two columns we have the names of the  $\gamma$ -ray source and its WISE counterpart. The last two columns show the AP as given by the LR and RF methods.

- Astropy Collaboration, Robitaille, T. P., Tollerud, E. J., et al. 2013, *A&A*, 558, A33, doi: [10.1051/0004-6361/201322068](https://doi.org/10.1051/0004-6361/201322068)
- Astropy Collaboration, Price-Whelan, A. M., Sipőcz, B. M., et al. 2018, *AJ*, 156, 123, doi: [10.3847/1538-3881/aabc4f](https://doi.org/10.3847/1538-3881/aabc4f)
- Atwood, W., Abdo, A. A., Ackermann, M., et al. 2009, *The Astrophysical Journal*, 697, 1071
- Breiman, L. 2001, *Machine learning*, 45, 5
- Chiaro, G., Salvetti, D., La Mura, G., et al. 2016, *Monthly Notices of the Royal Astronomical Society*, 462, 3180
- Crespo, N. Á., Massaro, F., Milisavljevic, D., et al. 2016, *The Astronomical Journal*, 151, 95
- D’Abrusco, R., Massaro, F., Ajello, M., et al. 2012, *The Astrophysical Journal*, 748, 68
- D’Abrusco, R., Massaro, F., Paggi, A., et al. 2013, *The Astrophysical Journal Supplement Series*, 206, 12
- . 2014, *The Astrophysical Journal Supplement Series*, 215, 14
- D’Abrusco, R., Crespo, N. Á., Massaro, F., et al. 2019, *The Astrophysical Journal Supplement Series*, 242, 4
- de Menezes, R., Peña-Herazo, H. A., Marchesini, E. J., et al. 2019, *Astronomy & Astrophysics*, 630, A55
- de Menezes, R., Amaya-Almazán, R. A., Marchesini, E. J., et al. 2020, *Ap&SS*, 365, 12, doi: [10.1007/s10509-020-3727-5](https://doi.org/10.1007/s10509-020-3727-5)
- Doert, M., & Errando, M. 2014, *The Astrophysical Journal*, 782, 41
- Fermi-LAT Collaboration, T., et al. 2019, arXiv preprint arXiv:1902.10045
- Fichtel, C., Bertsch, D., Chiang, J., et al. 1994, *The Astrophysical Journal Supplement Series*, 94, 551
- Hassan, T., Mirabal, N., Contreras, J., & Oya, I. 2012, *Monthly Notices of the Royal Astronomical Society*, 428, 220
- James, G., Witten, D., Hastie, T., & Tibshirani, R. 2013, *An introduction to statistical learning*, Vol. 112 (Springer)
- Kovačević, M., Chiaro, G., Cutini, S., & Tosti, G. 2019, *Monthly Notices of the Royal Astronomical Society*, 490, 4770
- Lefaucheur, J., & Pita, S. 2017, *Astronomy & Astrophysics*, 602, A86
- Marchesini, E., Peña-Herazo, H., Crespo, N. Á., et al. 2019, *Astrophysics and Space Science*, 364, 5
- Masci, F. J., Condon, J., Barlow, T., et al. 2001, *Publications of the Astronomical Society of the Pacific*, 113, 10
- Massaro, E., Maselli, A., Leto, C., et al. 2015a, *Astrophysics and Space Science*, 357, 75
- Massaro, F., D’Abrusco, R., Ajello, M., Grindlay, J., & Smith, H. A. 2011, *The Astrophysical Journal Letters*, 740, L48
- Massaro, F., D’Abrusco, R., Landoni, M., et al. 2015b, *The Astrophysical Journal Supplement Series*, 217, 2
- Massaro, F., Crespo, N. Á., D’Abrusco, R., et al. 2016, *Astrophysics and Space Science*, 361, 337
- Mirabal, N., Frias-Martinez, V., Hassan, T., & Frias-Martinez, E. 2012, *Monthly Notices of the Royal Astronomical Society: Letters*, 424, L64
- Nolan, P. L., Abdo, A., Ackermann, M., et al. 2012, *The Astrophysical Journal Supplement Series*, 199, 31
- Parkinson, P. S., Xu, H., Yu, P., et al. 2016, *The Astrophysical Journal*, 820, 8
- Pedregosa, F., Varoquaux, G., Gramfort, A., et al. 2011, *Journal of Machine Learning Research*, 12, 2825
- Peña-Herazo, H., Massaro, F., Chavushyan, V., et al. 2019, *Astrophysics and Space Science*, 364, 85
- Peña-Herazo, H. A., Marchesini, E. J., Crespo, N. Á., et al. 2017, *Astrophysics and Space Science*, 362, 228
- Richter, G. 1975, *Astronomische Nachrichten*, 296, 65
- Salvetti, D., Chiaro, G., La Mura, G., & Thompson, D. J. 2017, *Monthly Notices of the Royal Astronomical Society*, 470, 1291
- Sutherland, W., & Saunders, W. 1992, *Monthly Notices of the Royal Astronomical Society*, 259, 413
- Taylor, M. B. 2005, *Astronomical Society of the Pacific Conference Series*, Vol. 347, TOPCAT & STIL: Starlink Table/VOTable Processing Software, ed. P. Shopbell, M. Britton, & R. Ebert, 29

The Fermi-LAT collaboration. 2019, arXiv e-prints,  
arXiv:1905.10771. <https://arxiv.org/abs/1905.10771>

Wolstencroft, R., Savage, A., Clowes, R., et al. 1986,  
Monthly Notices of the Royal Astronomical Society, 223,  
279